arXiv:1210.8450v1 [quant-ph] 31 Oct 2012

Quantum transport with coupled cavities on the Apollonian network

G. M. A. Almeida and A. M. C. Souza*
Departamento de Física, Universidade Federal de Sergipe, 49100-000 São Cristóvão, Brazil

(Dated: November 1, 2012)

We study the dynamics of atomic and photonic excitations in the Jaynes-Cummings-Hubbard (JCH) model when each cavity occupies the nodes of an Apollonian network (AN). Such structure shows small-world and scale-free properties, and has been investigated within many physical models. By numerically diagonalizing the system Hamiltonian in the single-excitation subspace, we evaluate the time evolution of an initial state prepared as an even superposition of both atomic and photonic modes fully localized at a specific node. For the large hopping regime we provide a detailed description of the quantum transport properties of the AN and show that the complex interplay between the many cavity-cavity degrees of freedom induces both extended and localized states varying periodically. The excitation is most likely to be found in the initial node and its propagation strongly depends on the initial conditions. We also discuss the strong atom-cavity coupling regime, where atomic and photonic modes propagates identically, and the JCH regime, where the system is allowed to roam between atomic and photonic degrees of freedom, since the hopping parameter and the atom-cavity coupling strength are of the same order. In this regime, different cavities contribute either to the atomic or photonic component mostly, depending on the initial conditions.

PACS numbers: 42.50.Pq, 42.50.Ex, 03.67.-a, 89.75.Da

I. INTRODUCTION

Cavity quantum electrodynamics systems have been widely considered as a suitable choice for implementation of quantum information processing schemes [1–3]. A very simple cavity system consists of a two-state atom coupled to a single mode of an electromagnetic field inside an ideal cavity. Such system is described by the well known Jaynes-Cummings (JC) model [4], which is exactly solvable and has been useful for investigating fundamental aspects of the interaction between light and matter. Further generalizations of the JC model include multiple atoms, N-level atom, dissipation, and so forth [5].

Experimental advances in optical microcavities [6], photonic crystals [7], and superconducting devices [8] has brought interest to Hubbard-like models where photons can hop through an array of coupled-cavity systems. In particular, the Jaynes-Cummings-Hubbard (JCH) model [9, 10] provides a new framework for studying many-body phenomena such as phase transitions where strongly correlated photons play the role. Most of recent work has focused on the Mott insulator-superfluid quantum phase transition of polaritons (combined atomic and photonic excitations) [11–13].

Coupled-cavity systems allow the control and measurement of individual nodes. Therefore, it also provides a reliable setup for distributed quantum information processing [14], which requires entanglement generation [15] and quantum state transfer between distant nodes in a network [16]. Recently, Ogden *et al.* [17] studied quantum state transfer between two coupled cavities, each one containing a single two-level atom. In terms of delocalized field modes, they have derived the dynamics on the single-excitation subspace for a variety of interaction regimes focusing on the atomic state transfer and found that, by setting the right parameters, one can achieve a high-fidelity state transfer without populating the field mode, thus avoiding photon loss. Makin *et al.* [18] considered a one-dimensional array of cavities and dealing with both atomic and photonic excitation dynamics they discussed the localized and delocalized behaviour of the system. They have also shown that by parabolically coupling the cavities, or encoding the initial state as a gaussian wave-packet, one can avoid pulse dispersion. In [19], Dong *et al.* discussed the binary transmission dynamics in a chain of coupled cavities, each one containing a tree-level atom and showed that a certain class of coding and decoding protocol can improve the transmission fidelity.

These results indicate that even in the single-excitation subspace the JCH model presents a rich dynamics due to the interplay between atomic and photonic degrees of freedom. Thus it would be interesting to apply this model to more complex structures. Lately, a class of networks which are neither completely regular nor completely random, named *small-world* networks [20], where the average length of the shortest path l between two nodes increases logarithmically with the network size N ($l \propto \ln N$), has been widely studied within many fields, from social and biological systems [20, 21] to classical and quantum transport dynamics [22–24]. In particular, a class of complex networks called Apollonian networks (AN) [25], which are simultaneously small-world, scale-free (that displays a power-law degree distribution), and can be embedded in Euclidean space, has brought some attention. The free-electron gas [26], magnetic models [27], tight-biding models [28], correlated electron systems [29], and quantum walks [30] in such networks have been investigated. AN's arise from the problem of space-filling packing of spheres [31]. It can be deterministic or ran-

---

* Electronic address: amcsouza@ufs.br

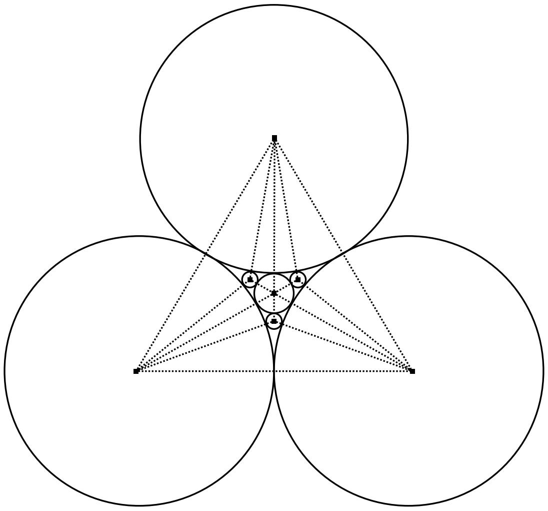

FIG. 1. The second generation ($n = 2$) Apollonian packing (solid lines) and the corresponding AN (dotted lines).

dom, and depends on the initial configuration. The most common packing starts with three mutually touching circles. The first generation, $n = 1$, is achieved by inserting a maximal circle in the interstice bounded by the three initial circles. Further generations are obtained by repeating this process for every empty space. This packing can be mapped to the AN as shown in Fig. 1. At a given generation, the number of nodes is given by $N(n) = (3^n + 5)/2$, and the number of connections by $C(n) = (3^{n+1}+3)/2$ ($n = 0, 1, 2, ...$). In each generation a new group of nodes sharing the same degree γ is created. More precisely, there are $3^{n-1}, 3^{n-2}, 3^{n-3}, ..., 3^2, 3, 1$, and 3 nodes with degree $\gamma = 3, 3 \cdot 2, 3 \cdot 2^2, ..., 3 \cdot 2^{n-2}, 3 \cdot 2^{n-1}$, and 2^n+1, respectively, where the last number represents the three corner nodes. The central node, often referred as the hub node, has the largest degree.

In this paper, we study the dynamics of the JCH model defined on the AN. We numerically diagonalize the Hamiltonian in the single-excitation subspace and and solve Schrödinger equation thus obtaining the time evolution of atomic and photonic occupation probability distribution for fully localized initial states prepared in an even superposition of atomic and photonic modes. We consider three different energy regimes. For large inter-cavity hopping, the photonic component propagates practically free, without significantly exchange energy with the atomic modes in short time scales. In this regime we analyse the photonic component transport through the AN when the initial state is prepared in different nodes and show how it changes by varying the network size. When the atom-cavity coupling strength dominates, we have a similar propagation dynamics but with both components travelling simultaneously. For comparable hopping and atom-cavity coupling, the dynamics turns out to be more complex since the system can roam between atomic and photonic degrees of freedom, thus leading to different dynamics.

In what follows, Sec. II, we introduce the JCH model. In Sec. III we present our numerical results for the time evolution at different energy regimes. Finally, in Sec. IV, we draw our conclusions.

II. THE JAYNES-CUMMINGS-HUBBARD MODEL

Let us consider a system of coupled cavities where each one occupies the nodes of an Apollonian network. A two-level system $\{|g\rangle, |e\rangle\}$ coupled to a single field mode can described by the JC Hamiltonian [4] (in the rotating wave approximation),

$$h_j^{JC} = \frac{\omega_a}{2}\sigma_z + \omega_f a_j^\dagger a_j + \beta(\sigma_j^+ a_j + \sigma_j^- a_j^\dagger), \qquad (1)$$

where $\sigma_z |g\rangle = -|g\rangle$ and $\sigma_z |e\rangle = |e\rangle$, σ_j^+ (σ_j^-) and $a_j^\dagger$ (a_j) are, respectively, the atomic and photonic raising (lowering) operators for cavity j, β is the atom-cavity coupling strength, ω_a the atomic transition frequency, ω_f the field mode frequency, and we set $\hbar = 1$ for convenience. If we include photon evanescent hopping between nearest-neighbour cavities (tight-binding approximation), we can represent the whole system by the JCH Hamiltonian

$$H = \sum_{j=1}^{N(n)} h_j^{JC} - \sum_{i,j=1}^{N(n)} \kappa A_{ij}^{(n)} a_i^\dagger a_j, \qquad (2)$$

where κ is the cavity-cavity coupling strength, $N(n)$ number of nodes for a fiven AN generation n, and $A_{ij}^{(n)}$ the adjacency matrix elements. We now restrict the system basis to the single-excitation subspace. These excitations can be photonic or atomic, that is $|Q\rangle |g, 1\rangle$ or $|Q\rangle |e, 0\rangle$, respectively, where $Q \in \{1, ..., N(n)\}$ specifies the cavity. Then the whole system state is written as the tensor product of every single-cavity state, where one excitation must be conserved (the other non-excited cavities are in the $|g, 0\rangle$ state), so the Hilbert space has $D = 2N(n) = 3^n + 5$ dimensions. In such basis, the matrix form of the Hamiltonian (2) can be simply expressed by [18]

$$H_{1\text{exc}} = \frac{\Delta}{2} I_{N(n)} \otimes Z + \beta I_{N(n)} \otimes X - \kappa \mathbf{A}_n \otimes \frac{I_2 + Z}{2}, \qquad (3)$$

where $\Delta = \omega_f - \omega_a$ is the detuning between photonic and atomic modes, I_m is the $m \times m$ identity matrix, X and Z are the usual Pauli matrices, and $\mathbf{A}_n$ the adjacency matrix. The ground state $\otimes_{Q=1}^{N(n)} |Q\rangle |g, 0\rangle$ is not included in this subspace, that is, the system is already set with the single-excitation.

The AN does not take geometrical deformations into account so we are only interested in the connections between the nodes. By considering uniform cavity-cavity coupling, the adjacency matrix $\mathbf{A}_n$ for $n = 2$, for exam-

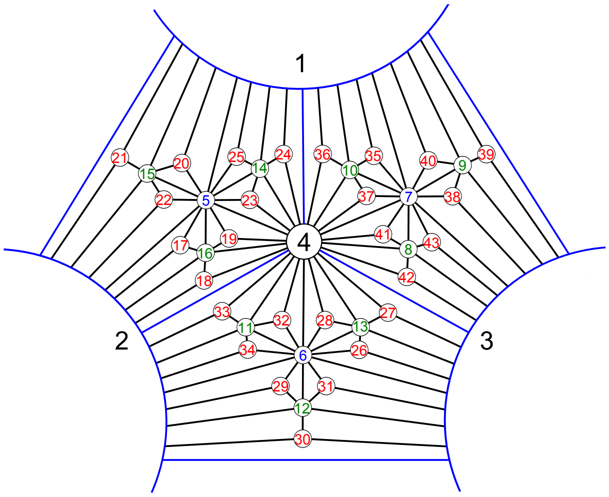

FIG. 2. (Color online) The Apollonian network for $n = 4$ (43 nodes). The first generation is made up by nodes 1 to 4, the second one includes 5 to 7, the third, 8 to 16, and the fourth, 17 to 43. The corner nodes were drawn bigger for a clearer visualization. This is the node labelling we will adopt through the paper.

ple, can be written by

$$A_2 = \begin{pmatrix} 0 & 1 & 1 & 1 & 1 & 0 & 1 \\ 1 & 0 & 1 & 1 & 0 & 1 & 1 \\ 1 & 1 & 0 & 1 & 0 & 0 & 0 \\ 1 & 1 & 1 & 0 & 1 & 1 & 1 \\ 1 & 0 & 0 & 1 & 0 & 0 & 1 \\ 0 & 1 & 0 & 1 & 0 & 0 & 1 \\ 1 & 1 & 0 & 1 & 1 & 1 & 0 \end{pmatrix} \tag{4}$$

(see Fig. 1). In order to discuss our results in next section, we need the appropriate identification of each node (cavity), then Fig. 2 provides the node numbering which we are going to consider herein, up to the 4th AN generation.

III. NUMERICAL RESULTS

In this section we display the results for time-evolution of the JHC model in the AN obtained by numerical diagonalization of the Hamiltonian (2) in the single-excitation subspace thus finding its eigenvalues E_j and the corresponding normalized eigenstates $|E_j\rangle$. We discuss the system dynamics for different energy regimes and consider no detuning, $\Delta = 0$, between photonic and atomic modes. We are mostly interested in the analysis of photonic and atomic excitation occupation probabilities in different cavities for a given initial state, namely $|\psi(0)\rangle$, through the time. The state at time t is given by $|\psi(t)\rangle = U(t)\,|\psi(0)\rangle$, where $U(t) = e^{-iHt}$ is the quantum time evolution operator. If the initial state is prepared in a equal superposition of photonic and atomic modes (i.e., a single-cavity eigenstate for $\Delta = 0$ [5]), $|\psi_k(0)\rangle = |k\rangle \otimes (|g,1\rangle + |e,0\rangle)/\sqrt{2}$ at node (cavity) k, we write

$$\pi^{ph}_{\ell k}(t) = \left| \sum_j^D e^{-iE_j t} \langle \psi_k(0)|E_j\rangle \langle E_j|\ell, g\rangle \right|^2 \tag{5}$$

and

$$\pi^{at}_{\ell k}(t) = \left| \sum_j^D e^{-iE_j t} \langle \psi_k(0)|E_j\rangle \langle E_j|\ell, e\rangle \right|^2 \tag{6}$$

as the probability of finding both photonic and atomic excitations, respectively, at node ℓ in time t, where we have denoted $|\ell, g\rangle \equiv |\ell\rangle\,|g,1\rangle$ and $|\ell, e\rangle \equiv |\ell\rangle\,|e,0\rangle$.

A. Large hopping regime

First, we investigate the large hopping regime ($\kappa \gg \beta$). In this case, the atom-cavity interaction slowly takes place so that the photonic excitation propagates practically free, while the atomic one does not "move" in short time scales. Remember that only the photons can hop while atoms remain stationary. The atomic component dynamics is then correlated to the photonic one, although not exactly the same, except when the atom-cavity coupling β dominates the hopping strength as we will see later.

The AN has a $2\pi/3$ rotational symmetry, hence there are several subsets of equivalent nodes (see Fig. 2) like $\{1, 2, 3\}$, $\{5, 6, 7\}$, $\{8, 10, 11, 13, 14, 16\}$, and so forth, in which $|\psi_k(0)\rangle$ would lead to the same dynamics. Likewise, for the initial state set at the hub node ($k = 4$), the occupation probabilities $\pi^{type}_{\ell 4}(t)$ are equal for each subset.

Figs. 3 and 4 show the time evolution of the photonic occupation probability $\pi^{ph}_{\ell k}(t)$, for different initial single-cavity eigenstates $|\psi_k(0)\rangle$, in the $n = 3$ and $n = 4$ AN, respectively. Although exhibiting a rather complex dynamics, we can identify some general aspects of the propagation. The most remarkable feature is periodic transition between localized and extended states. The return probability $\pi^{ph}_{kk}(t)$ can reach the highest values so that the excitation is most likely to be found in the initial node. This localization is stronger for $k = 4$, the hub node. Also, it seems that $\pi^{ph}_{kk}(t)$ oscillates faster for the initial state set at nodes with a higher degree of freedom γ. In Fig. 5 we plot $\pi^{ph}_{44}(t)$ (solid line) and also the atomic component $\pi^{at}_{44}(t)$ (dotted line) time evolution in detail. As we said before the atomic mode barely moves, except for small oscillations (see inset of Fig. 5) due to the photonic component behaviour. Since the atom-cavity interaction process has much lower associated energies, only the cumulative effect of these interactions in longer time scales may significantly vary $\pi^{at}_{\ell k}(t)$. Therefore, at

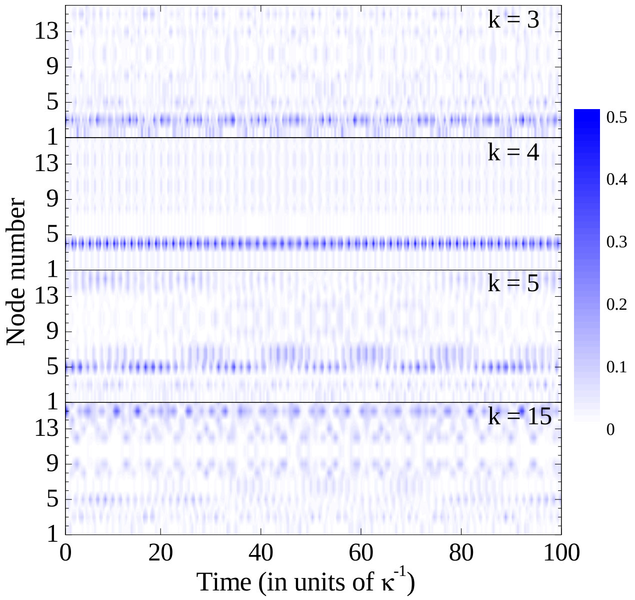

FIG. 3. (Color online) Time evolution of the photonic excitation $\pi_{\ell k}^{ph}(t)$ through the $n = 3$ AN (16 nodes) for the large hopping regime. The vertical axis represents the occupation probability of a particular node (cavity). The single-cavity initial state $|\psi_k(0)\rangle = |k\rangle \otimes (|g,1\rangle + |e,0\rangle)/\sqrt{2}$ is prepared at nodes $k = 3$, 4, 5, and 15. System parameters are $\kappa/\beta = 10^3$ and $\Delta = 0$. The node numbering is available in Fig. 2.

the large hopping regime we shall focus on the photonic mode propagation dynamics thus aiming to explain the quantum transport properties of the AN.

Now let us turn our attention to the probability of finding the excitation in nodes other than the initial one. In general, such probabilities are very small compared to $\pi_{kk}(t)$, although they can reach relevant values in some specific nodes. The overall probability distribution strongly depends on the AN generation and the initial conditions. In Fig. 3, by examining $\pi_{\ell k}(t)$ for $k = 3$, we see that a significant amount of probability flows to the other nodes belonging to the same degree group, that is 1 and 2 (check Fig. 2 for node numbering). The same applies to $\pi_{65}(t)$ and $\pi_{75}(t)$ when $k = 5$. For $k = 15$, the nodes 10 and 11 even belonging to the same degree group are barely populated. It suggests that sharing the same degree does not necessarily imply in privileged networking. It turns clearer in Fig. 4 for $k = 18$ and 21, where the excitation is mostly spread to a few nodes within the subnetwork [32] generated by the new corner nodes 1, 2, and 4. When $k = 5$ for $n = 4$ (Fig. 4), the excitation still roams between nodes 6 and 7, but now avoiding transport to higher generation nodes. For $k = 15$ in Fig. 4, there is a relevant probability of finding the excitation at nodes 20, 21, and 22. These nodes belong to the subnetwork formed by nodes 1, 2, and 5, where the node 15 play the role of hub node. These observations indicate that these subnetworks has a fundamental part on the system transport dynamics for higher AN generations.

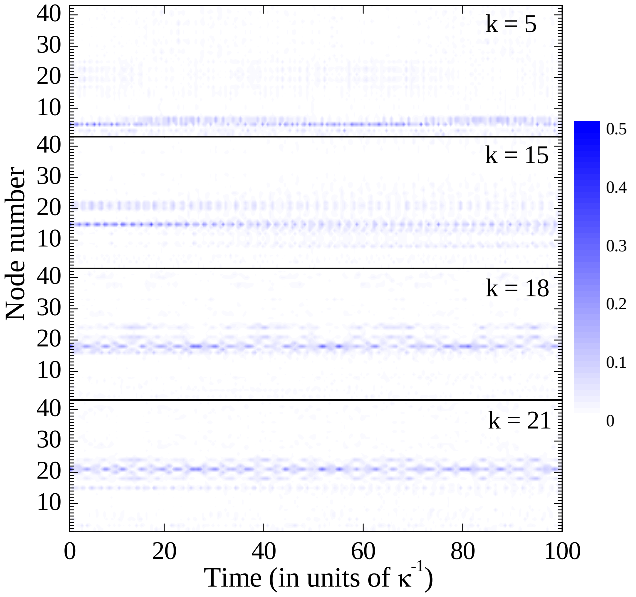

FIG. 4. (Color online) Same as Fig. 3 but for $n = 4$ (43 nodes) and $k = 5$, 15, 18, and 21.

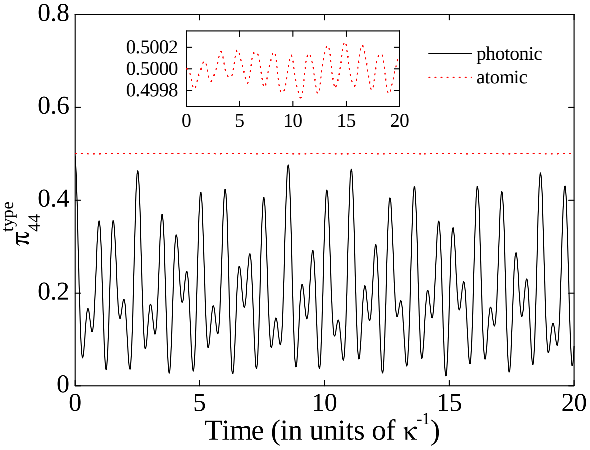

FIG. 5. (Color online) Photonic (solid line) and atomic (dotted line) return probabilities for the initial state prepared in $|\psi_4(0)\rangle$ at the $n = 4$ AN. The inset shows small oscillations in $\pi_{44}^{at}(t)$ induced by the photonic mode propagation. System parameters are $\kappa/\beta = 10^3$ and $\Delta = 0$.

A better way to visualize how the excitation probability distributes between the nodes for given initial conditions is by calculating the long time average of $\pi_{\ell k}^{ph}(t)$ defined as

$$\begin{aligned}\chi_{\ell k}^{ph} &= \lim_{T\to\infty} \frac{1}{T}\int_0^T \pi_{\ell k}^{ph}(t)dt \\ &= \sum_{i,j} \delta(E_i - E_j)\,\langle \ell, g|E_i\rangle\,\langle E_i|\psi_k(0)\rangle \times \\ &\times \langle \psi_k(0)|E_j\rangle\,\langle E_j|\ell, g\rangle\,, \qquad (7)\end{aligned}$$

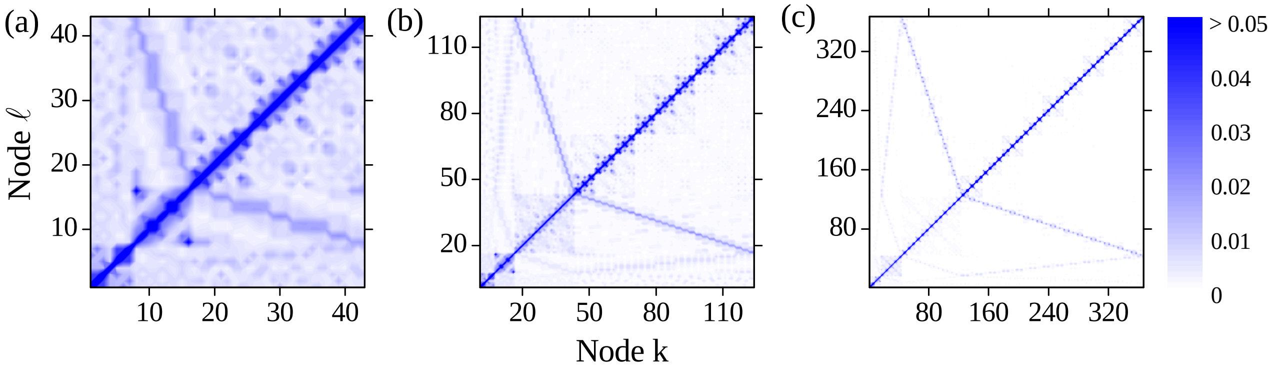

FIG. 6. (Color online) Photonic long-time average occupation probabilities $\chi^{ph}_{\ell k}$ for (a) $n = 4$ (43 nodes), (b) $n = 5$ (124 nodes), and (c) $n = 6$ (367 nodes). System parameters are $\kappa/\beta = 10^3$ and $\Delta = 0$. The plot shape is symmetrical since $\chi^{ph}_{\ell k} = \chi^{ph}_{k\ell}$ for every k and ℓ, and the highest values are χ^{ph}_{kk}, i.e., the average return probability. Although we have not provided the node numbering for nodes from generations higher than $n = 4$, the purpose here is to give an idea of how the subnetworks and nodes from different generations are connected among themselves. In each generation above, the darkest branch represents the average excitation transport probability between nodes belonging to the current generation and to the previous one. The square boundaries point out connections between nodes having the same degree.

where $\delta(E_i - E_j) = 1$ for $E_i = E_j$ and $\delta(E_i - E_j) = 0$ else. Fig. 6 shows the distribution of this average for different AN generations. First of all, notice that $\chi^{ph}_{\ell k} = \chi^{ph}_{k\ell}$ for every k and ℓ (since the evolution is unitary), hence this quantity provides us a clearer view on the way the nodes stablish communication channels with each other. As it must be, the higher averages are χ^{ph}_{kk}, however, by looking at the other connections we can identify several zones (square boundaries) and branches apart which, interestingly, present self-similarity as n increases. The branches connect generations with each other while the zones connect nodes from the same generation, i.e., with same degree γ. The strongest (darkest) branch is always the one connecting nodes from the current generation to the previous one. It mostly represents the links between the corresponding hub nodes from the 3^{n-2} subnetworks having 7 nodes, to its three nearest-neighbour nodes with $\gamma = 3$. As n increases, the previous branches still remain but with lower intensities since the aforementioned hub nodes now have a higher γ. Also, nodes from "distant" generations seem to be barely connected. This is because, when preparing the initial state in nodes from a current generation, the excitation is mostly roams between the initial node, other nodes with same degree belonging to local subnetworks, and its corresponding hub node from the previous generation. Notice in Fig. 6 that connections between nodes from the same generation are only relevant within subnetworks composed up to 16 nodes. For instance, at a given generation n there are 3^{n-m} subnetworks having $(3^m + 5)/2$ nodes. Needless to say, these degree interconnections also become weaker as generation increases.

Before discuss other energy regimes it would be useful to explain the reason for why the state always carries relevant information about its initial conditions by evaluating the participation ratio of eigenstates defined as

$$\xi_j = \frac{1}{\sum_{s=\{g,e\}} \sum_{i=1}^{N(n)} |\langle i, s|E_j\rangle|^4}, \tag{8}$$

for a given AN generation n. This quantity can assume values within 1, for completely localized states, and D, for extended states ($\langle i, s|E_j\rangle = 1/\sqrt{D}$ for all i). Fig. 7 shows the relationship between ξ_j/N and the probability of finding the system in each eigenstate, $|\langle E_j|\psi_k(0)\rangle|^2$, for a given initial condition $|\psi_k(0)\rangle$ [Fig. 7(a)], and the associated eigenvalues E_j [Fig. 7(b)], for the $n = 4$ AN. When we prepare $|\psi_k(0)\rangle$ in the hub node $k = 4$ (with degree $\gamma = 24$), the two most localized eigenstates (with $\xi_j/D \approx 0.05$), one being related to atomic excitation $|4, e\rangle$ ($E_j/\kappa \approx 0$) and the other to the photonic excitation $|4, g\rangle$ (the highest eigenvalue), become more populated thus strongly leading the system dynamics. Only a few other eigenstates, not much localized, gives a relevant contribution to the dynamics. Since we are considering the large-hopping regime, the atom-cavity interaction energies are very low so we clearly identify the middle range of eigenvalues ≈ 0 [see Fig. 7(b)] as being those belonging mostly to the atomic component of the system. In Fig. 7(a), as we set $|\psi_k(0)\rangle$ for nodes having lower degrees of freedom, for instance, $k = 3$, 5, and 21, where $\gamma = 17$, 12, and 3, respectively, the contribution from localized eigenstates decreases and then more extended states start to participate on the dynamics. Also, the eigenstates which mostly contribute to $\pi^{ph}_{kk}(t)$ has lower associated energy levels for smaller γ. It shows that the oscillation period of the return probability depends on γ, as we have already mentioned.

More details about localized and extended states on the AN and its relationship with the structure charac-

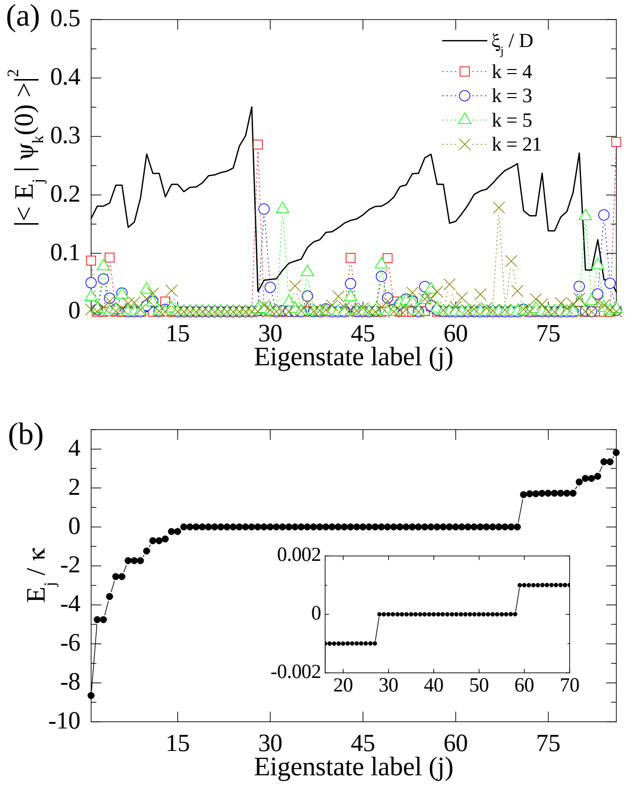

FIG. 7. (Color online) (a) The normalized participation rate of eigenstates ξ_j/D (solid line) and the probability of finding the system in eigenstate $|E_j\rangle$, that is $|\langle E_j|\psi_k(0)\rangle|^2$, for $k = 4$, 3, 5, and 21. System parameters are $n = 4$ (43 nodes), $\kappa/\beta = 10^3$, and $\Delta = 0$. The eigenstates are labeled according to increasing energy values and, within each degenerate group, by increasing values of ξ_j. (b) The corresponding energy values (in units of κ^{-1}). The energy levels around zero is shown on the inset. Actually, the ones lying at the middle range (≈ 0) are not all degenerate. These energy levels arise from the atomic modes and since $\kappa \gg \beta$, its energy scale is very small compared to the photonic counterpart.

teristic spectrum and symmetry properties can be found in Ref. [28], where they considered a simple tight-biding electronic model. The tendency of the excitation for staying in the initial node has been found for the continuous-time quantum walk in the same structure [30], and also in a small-world network defined by adding random links in a one-dimensional ring of nodes [24]. By increasing the number of additional bonds, they have shown that this effect becomes stronger thus avoiding dispersion.

B. The JCH and strong atom-cavity coupling regimes

In what follows we consider the situation where the coupling between cavities and the atom-cavity interaction strength are of the the same order ($\kappa \approx \beta$). That is the energy regime where the JCH model displays its full nature. In this case, as the photonic excitation propagates through the network it exchanges energy with the atomic modes in such a way that the whole system starts to roam between photonic and atomic degrees of freedom. Each cavity provides its contribution to mostly either one of these two components, depending on the system initial conditions and the characteristic single-cavity energy levels in a rather complex way. Since a fully localized initial state of the form $|\psi_k(0)\rangle$ mostly leads the excitation to return to the initial node, we presume that the oscillation rate of π_{kk}^{type} will be primarily relevant for driving the whole system among the atomic and photonic degrees of freedom. Fig. 8 gives an idea of how the initial state may significantly changes the way both modes contribute to the system dynamics in such energy regime. In Fig. 8(a) we show the long-time average occupation probability distribution $\chi_{\ell k}^{type}$ when $|\psi_k(0)\rangle$ is set at the hub node, $k = 4$. Notice that $\chi_{k\ell}^{at}$ can be evaluated by the same way as Eq. 7 by projecting the eigenstates on $|\ell, e\rangle$, instead of $|\ell, g\rangle$. We can see that some groups of nodes have higher $\chi_{\ell 4}^{ph}$ values (including the hub node), others mostly contribute to $\chi_{\ell 4}^{at}$, and a few practically contributes with the same amount for both components. In Fig. 8(b) we plot the time evolution of the probability of finding the photonic and atomic excitation at any cavity by summing $\pi_{\ell 4}^{type}$ over ℓ. In this case, the system notoriously fluctuate between both components. It results mainly from the fast oscillation rate of π_{44}^{ph} (since the hub node has the higher γ) combined with the strong localization properties. The average values are $\chi_{44}^{ph} \approx 0.26$ and $\chi_{44}^{at} \approx 0.14$ hence representing a great difference. Figs. 8(c) and 8(d) show the same quantities but now for $k = 18$ ($\gamma = 3$). The higher averages $\chi_{\ell 18}^{type}$ does not differ much for both types, thus resulting in small variations of $\sum_\ell \pi_{\ell 18}^{type}$.

In summary, at the large hopping regime, $\kappa \gg \beta$, the interplay between atomic and photonic degrees of freedom is minimal so that the atomic excitation only significantly propagates in larger time scales. Thus the cavity-cavity coupling parameter, κ, allows the control of the atomic mode velocity. When the JCH regime ($\kappa \approx \beta$) takes place, atomic and photonic degrees of freedom start to interfere with each other, thus resulting in different dynamics . We can keep on decreasing κ/β until reaching the strong atom-cavity coupling regime, where photonic and atomic components have exactly the same dynamics. This regime transition is clearly shown on Fig. 9 where we plot the time evolution of the photonic [Fig. 9(a)] and atomic [Fig. 9(b)] return probabilities π_{44}^{type} for a large range of κ/β values from 10^3 to 10^{-3}. At the $\kappa \ll \beta$ regime, the dynamics for both atomic and photonic modes behaves exactly like at the large hopping regime but now creating new single-cavity eigenstates (if the initial state is prepared in $|\psi_k(0)\rangle$) as passing by other cavities, and propagating at half the speed of the photonic excitation at the $\kappa \gg \beta$ regime [18]. Due to the fact that the atoms inside the cavities does not actually move, there is a small delay, namely δ, which tends to dis-

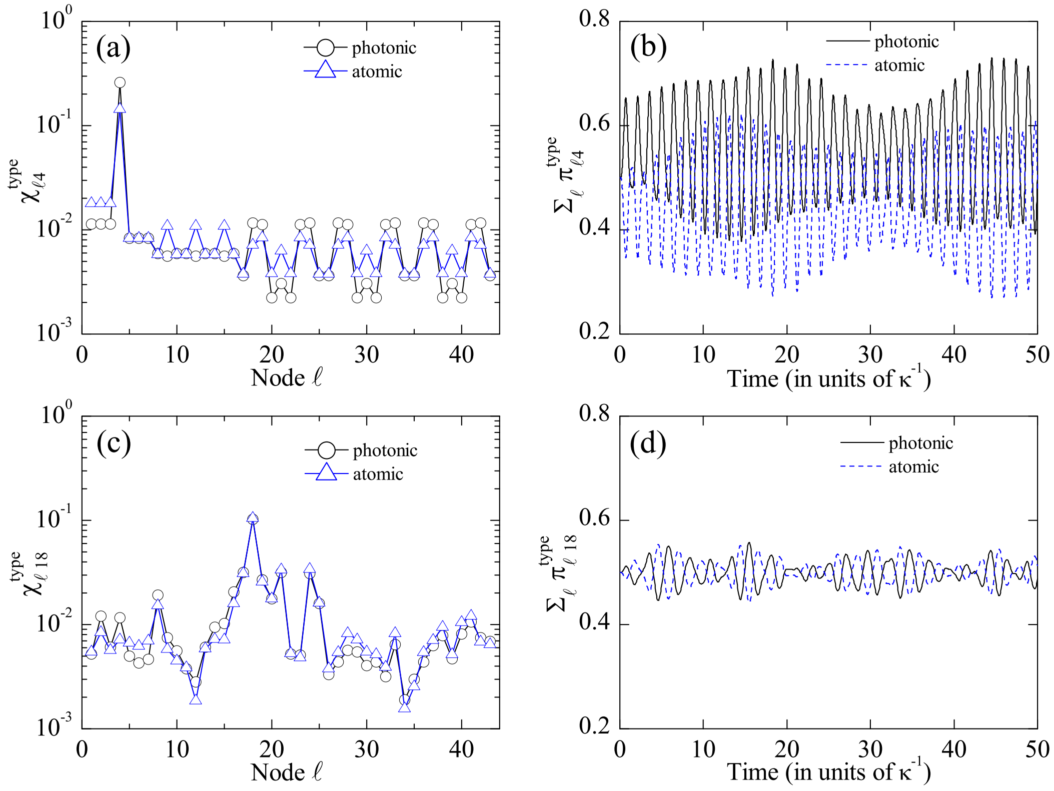

FIG. 8. (Color online) Figures (a) and (c) shows the photonic and atomic long-time average occupation probability distribution for $k = 4$ and $k = 18$, respectively, and (b) and (d), the corresponding time-dependent probability of finding both excitation types at any cavity, $\sum_\ell \pi_{\ell k}^{type}$. System parameters are $n = 4$, $\kappa/\beta = 1$, and $\Delta = 0$. The return average probabilities are $\chi_{44}^{ph} \approx 0.26$, $\chi_{44}^{at} \approx 0.14$, $\chi_{1818}^{ph} \approx 0.103$, and $\chi_{1818}^{at} \approx 0.105$.

turb the single-cavity eigenstates, but $\delta \to 0$ as $\kappa/\beta \to 0$. By the same way, at the large hopping regime, $\delta \to \infty$ as $\kappa/\beta \to \infty$ thus freezing the atomic component.

IV. CONCLUSIONS

Even at the single-excitation subspace, the JCH model provides a rich dynamics. In addition, the Apollonian network has ubiquitous transport features. We studied the propagation dynamics by considering the initial state as an even superposition of atomic and photonic modes fully localized in some specific node. At the large hopping regime, where practically only the photonic component moves, we focused the analysis on the quantum transport dynamics in the AN. In such structure, the excitation is most likely to be found at the initial node due to the characteristic network spectrum properties. By evaluating the long time average photonic occupation probability for different AN generations, we have discussed the interplay between the nodes and subnetworks thus showing their role on the system dynamics. At a given generation n, the nodes with $\gamma = 3$ are mostly connected with its correspondent hub node from the previous generation and with some other nodes having the same degree within local subnetworks. These properties are also valid for any analogue tight-binding model in the same AN.

At the JCH regime, where the hopping term and the atom-cavity coupling strength are of the same order, we have shown that each cavity gives its own contribution for the atomic and photonic modes thus inducing the system to roam between these two degrees of freedom. When the atom-cavity coupling term dominates, the excitation propagates maintaining the even superposition of atomic and photonic modes (the single-cavity eigenstate).

Even though high-fidelity excitation transport protocols in an one-dimensional chain of coupled cavities has been proposed [18, 19], such regular structures have strong dispersive properties, in contrast to the AN, where we have shown that the excitation actually avoids propagating to some specific nodes, even when it is a first-neighbour node, without any coding-decoding protocol. In fact, we have only dealt with the most simple fully localized entangled initial state. Obviously, there are several possible combinations of initial states that should generate different and much more complex dynamics.

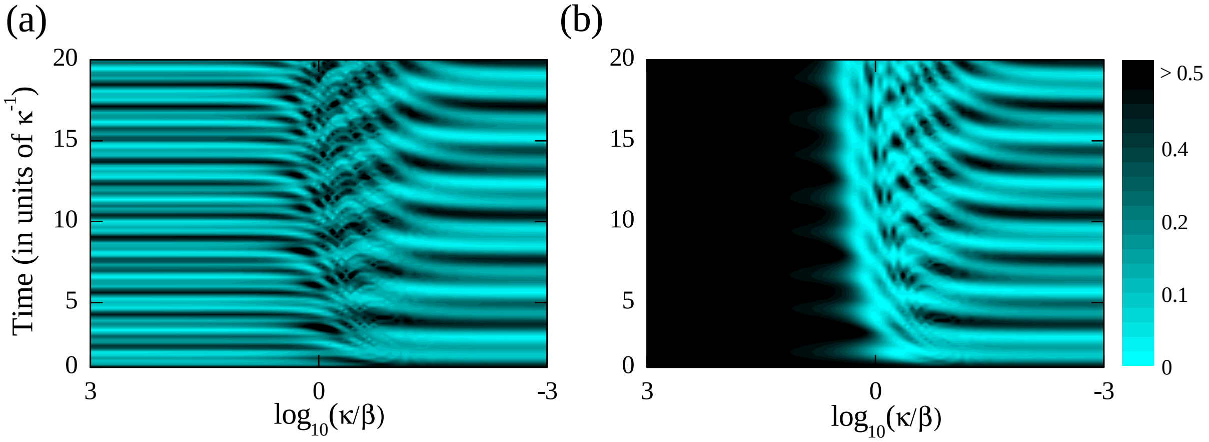

FIG. 9. (Color online) Comparison between atomic and photonic propagation dynamics from the large hopping regime $\kappa/\beta = 10^3$ to the strong atom-cavity coupling regime $\kappa/\beta = 10^{-3}$. In (a), the photonic return probability to the hub node, π_{44}^{ph}, and in (b) the atomic counterpart. System parameters are $n = 4$ and $\Delta = 0$. The middle range of κ/β values is where the JCH model plays its main role.

ACKNOWLEDGEMENTS

This work was supported by the CNPq (Brazilian agency). A.M.C.S. wishes to thank the National Institute of Science and Technology for Complex Systems.

[1] M. A. Nielsen and I. L. Chuang, *Quantum Computation and Quantum Information* (Cambridge University Press, 2000).

[2] J. Pachos and H. Walther, Phys. Rev. Lett. **89**, 187903 (2002).

[3] C.-H. Su, A. D. Greentree, W. J. Munro, K. Nemoto, and L. C. L. Hollenberg, Phys. Rev. A **78**, 062336 (2008).

[4] E. T. Jaynes and F. W. Cummings, in *Proc. of the IEEE*, Vol. 51 (1963) p. 89.

[5] B. W. Shore and P. L. Knight, J. Mod. Optics **40**, 1195 (1993).

[6] D. K. Armani, T. J. Kippenberg, S. M. Spillane, and K. J. Vahala, Nature (London) **421**, 925 (2003).

[7] K. Hennessy, A. Badolato, M. Winger, D. Gerace, M. Atatue, S. Gulde, S. Falt, E. L. Hu, and A. Imamoglu, Nature (London) **445**, 896 (2007).

[8] A. Wallraff, D. I. Schuster, A. Blais, L. Frunzio, R. S. Huang, J. Majer, S. Kumar, S. M. Girvin, and R. J. Schoelkopf, Nature (London) **431**, 162 (2004).

[9] M. J. Hartmann, F. G. S. L. Brandão, and M. B. Plenio, Nat. Phys. **2**, 849 (2006).

[10] A. D. Greentree, C. Tahan, J. H. Cole, and L. C. L. Hollenberg, Nat. Phys. **2**, 856 (2006).

[11] J. Koch and K. Le Hur, Phys. Rev. A **80**, 023811 (2009).

[12] S. Schmidt and G. Blatter, Phys. Rev. Lett. **103**, 086403 (2009).

[13] M. Hohenadler, M. Aichhorn, S. Schmidt, and L. Pollet, Phys. Rev. A **84**, 041608 (2011).

[14] J. I. Cirac, A. K. Ekert, S. F. Huelga, and C. Macchiavello, Phys. Rev. A **59**, 4249 (1999).

[15] D. G. Angelakis and S. Bose, J. Opt. Soc. Am. B **24**, 266 (2007).

[16] J. I. Cirac, P. Zoller, H. J. Kimble, and H. Mabuchi, Phys. Rev. Lett. **78**, 3221 (1997).

[17] C. D. Ogden, E. K. Irish, and M. S. Kim, Phys. Rev. A **78**, 063805 (2008).

[18] M. I. Makin, J. H. Cole, C. D. Hill, A. D. Greentree, and L. C. L. Hollenberg, Phys. Rev. A **80**, 043842 (2009).

[19] Y.-L. Dong, S.-Q. Zhu, and W.-L. You, Phys. Rev. A **85**, 023833 (2012).

[20] D. J. Watts and S. H. Strogatz, Nature (London) **393**, 440 (1998).

[21] M. E. J. Newman, Phys. Rev. E **64**, 016132 (2001).

[22] V. Latora and M. Marchiori, Phys. Rev. Lett. **87**, 198701 (2001).

[23] B. J. Kim, H. Hong, and M. Y. Choi, Phys. Rev. B **68**, 014304 (2003).

[24] O. Mülken, V. Pernice, and A. Blumen, Phys. Rev. E **76**, 051125 (2007).

[25] J. S. Andrade, H. J. Herrmann, R. F. S. Andrade, and L. R. da Silva, Phys. Rev. Lett. **94**, 018702 (2005).

[26] I. N. de Oliveira, F. A. B. F. de Moura, M. L. Lyra, J. S. Andrade, and E. L. Albuquerque, Phys. Rev. E **79**, 016104 (2009).

[27] R. F. S. Andrade and H. J. Herrmann, Phys. Rev. E **71**, 056131 (2005).

[28] A. L. Cardoso, R. F. S. Andrade, and A. M. C. Souza, Phys. Rev. B **78**, 214202 (2008).

[29] A. M. C. Souza and H. Herrmann, Phys. Rev. B **75**, 054412 (2007).

[30] X.-P. Xu, W. Li, and F. Liu, Phys. Rev. E **78**, 052103 (2008).
[31] D. W. Boyd, Canadian Journal of Mathematics **25**, 303 (1973).
[32] The AN has a self-similar structure where each subnetwork, generated by 3 new corner nodes, locally preserves the AN recurrence but breaks the degree group symmetry of the original AN (see Fig. 2).